Research Article **AJGRR (2022) 6:20**

American Journal of Geographical Research and Reviews

(ISSN:2577-4433)

Remote sensing identification of early planting information of rapeseed in mountainous areas

Lulu Dong[1], Xin Zhang[1,2*], Wen Dong[2]

[1]School of Earth Science and Engineering, Hebei University of Engineering, Handan, China.

[2]State Key Laboratory of Remote Sensing Science, Aerospace Information Research Institute, Chinese Academy of Sciences, Beijing, China.

Fund item: The work was financially supported by digital Map of Chongqing Agricultural Industry (No. 21C00346), Key Science and Technology Special Fund of Inner Mongolia (No. 2021ZD0045), and Key Research and Development Program of Hainan Province (No. ZDYF2021SHFZ105).

ABSTRACT

As a major oilseed crop with high ornamental value, Accurate and timely determination of their distribution and area under cultivation is essential to ensure food security and achieve sustainable development goals. The bright yellow flowers are a unique feature of rapeseed compared to other crops. Therefore, the yellow flower index was previously used to detect rapeseed on aerial images or medium-resolution satellites. However, the impact of its unique topographic terrain structure confuses crop planting structure, while the yellow flower signal of rapeseed is weak in the early stage of rapeseed growth. Therefore, it remains challenging to accurately identify early rapeseed in the southwest mountains. In this study, a new mountain rape index (MWRI) is proposed based on Sentinel-2 time series images. First, the NDVI characteristics of vegetation were used to filter out non-vegetated areas. Secondly, the weak rapeseed signal of non-pure image elements was enhanced by combining the time series reflection variation curves of rapeseed in red, green, NIR, and SWIR bands. The MRM method was used to extract the rapeseed cultivation in Chongqing, a typical mountainous rapeseed growing area in China. Three different previously proposed rapeseed indices: normalized difference yellowness index (NDYI), and yellowness index (RYI) were also calculated for comparison, and validation using high-resolution image interpretation samples in Google earth showed that MWRI has higher rapeseed recognition accuracy OA above 0.97, while other rapeseed indices OA between 0.9 and 0.95. The results indicate that MWRI is an effective index to distinguish mountain rapeseed from other crops.

Keywords: Rapeseed mapping, Time-series optical satellite imagery, Mountainous areas

***Correspondence to Author:**

Xin Zhang[1, 2]

[1]School of Earth Science and Engineering, Hebei University of Engineering.

[2]State Key Laboratory of Remote Sensing Science, Aerospace Information Research Institute, Chinese Academy of Sciences.

How to cite this article:

Lulu Dong, Xin Zhang, Wen Dong. Remote sensing identification of early planting information of rapeseed in mountainous areas. American Journal of Geographical Research and Reviews, 2022, 6:20

eSciPub LLC, Houston, TX USA.

Website: https://escipub.com/

1. Introduction

As the third largest oilseed crop after oil palm and soybean, rapeseed is a major source of edible oil for human consumption and one of the renewable biological feedstocks for the petrochemical industry [1]. In addition, China discovered the ornamental value of rapeseed, which has largely contributed to local tourism development [2] [3]. However, domestic rapeseed production is far from self-sufficient, and rapeseed imports account for a quarter of the demand for important oilseeds [4]. Accurate identification of rapeseed planting information is important for the development of food and oil security and modernized precision agriculture in China.

Remote sensing has become a powerful tool for mapping the area and yield of rapeseed due to the wide coverage and regularity of image acquisition. Compared with other crops and vegetation types, rapeseed flowers are a unique feature of rapeseed. Therefore, some previous studies have used remote sensing to detect information on rapeseed in flat terrain areas. For example, Sulik et al [5] found a good correlation between the yellowness index (RYI) and yellow flower density of rapeseed in 2015. Sulik et al [6] further proposed the normalized yellowness index (NDYI) to predict rapeseed yield in 2016. Fang et al [7] demonstrated that the green band in UAV images is a good indicator for estimating rapeseed flowers. These studies showed the potential of green color in detecting yellow flowers of rapeseed. In addition, Shen et al. found that yellow flowers can reduce vegetation index values [8]. Therefore, Tao [9] used the EVI differences between the flowering and pre-flowering stages of rapeseed to map the distribution of rapeseed in the middle reaches of the Yangtze River. To address the spatial and temporal differences in rape flowering, Ashourloo et al [10] proposed to detect flowering time using inflection points in the time series of the sum of red and green bands. Han et al [11] proposed to determine the peak flowering time of rape using the local maximum of the NRFI (standardized rape flowering index) time series. These studies showed the important role of the red band in detecting the peak flowering of rapeseed. In general, these methods are feasible in most regions by mining the spectral properties of the canopy of rapeseed during flowering.

However, obtaining continuous and complete spatial distribution information in cloudy and rainy mountainous areas is hindered, so the robustness of spectral and phenological-based methods is broken. To fill in the missing data, smoothing and time series fill algorithms (e.g. Savitzky-Golay and Whittaker Smoother et al.) have been used for crop identification [12]. However, reconstruction of time-series crop profiles from filter-smoothed generated fill data may incorrectly recover crop-specific phenological patterns and is therefore not suitable for rapeseed mapping, which is very sensitive to flowering time. Although the MODIS rapeseed signal can be augmented with enhanced vegetation indices to obtain a large range of historical rapeseed planting information [11], such coarse image elements cannot meet the needs of modern precision agriculture. Another solution to improve data availability is the application of microwave remote sensing, however, limited and insufficient microwave data hinders the wide application of these data in long-term crop identification. The complex cropping structure of mountainous areas makes the applicability of most of the research methods for canopy reflection information of rape to mountainous areas uncertain.

To meet the needs of rapeseed monitoring and yield prediction, rapeseed identification results need to be obtained as early as possible[13]. However, how to extend the time window of

rapeseed mapping from significant flowering to pre-flowering is the key to early rapeseed identification.

Advances in high-performance cloud computing technology have facilitated huge leaps in the efficiency and accuracy of remote sensing data analysis. the GEE cloud computing platform provides the computing power to support the calculation of Sentinel-2 imagery and grain-oil crop mapping. In addition, GEE's code and methods are easy to share and reduce duplication.

To address these problems of rapeseed identification in mountainous areas, this paper combines the advantages of phenology and machine learning methods and proposes a method for high-precision oilseed rape mapping in mountainous areas using time-series optical satellite images. Firstly, based on the spectral and phenological characteristics, the weak oilseed rape signal of the Mountain Winter Rape Index (MWRI) enhanced image element is designed, which effectively improves the distinguishability of rapeseed from winter wheat by using the change of rapeseed phenological period. Secondly, a multi-subtype fusion framework was constructed to achieve accurate identification of rapeseed GEE in complex environments in mountainous areas.

2. Study areas and data

2.1 Study areas

China's rapeseed is concentrated in the Yangtze River basin and is also known as winter rapeseed due to the difference in vernalization time and temperature [14]. By considering the availability of field data and the applicability of the proposed method in the environment, two sites in Chongqing city in the Yangtze River basin were selected for the experiment in this study, as shown in Figures 1(a) and 1(b). Site A (Fig. 1(a)) is located within the Hechuan district of Chongqing city, with an area of about 106 m^2 and a subtropical monsoon climate with an annual precipitation of 400-600 mm, which is one of the commercial grain bases in China. The topography of the Hechuan district is mainly hilly, with many flat dams along the coast. The main cultivated crops are rape, winter rice, winter wheat, corn, soybeans, and vegetables. Site B (Figure 1(b)) is located in Zhong County, Chongqing, with an area of about 102 square kilometers. Zhong County has steep valley slopes due to the relative height difference of the river valley above 700 m. The vegetable species are sparse compared with Site A. The food and oil crops mainly include winter rape, winter wheat, and rice, among which the value of rape is mainly for ornamental and oil extraction.

All of the above study sites have artificially irrigated rape fields with different varieties of rape. The sowing dates of the fields within the study sites varied according to the environmental conditions, the competent decisions of the farmers, and some other factors [15]. The use of google earth (https://www.google.com/earth) aided in the identification of the phenological stages of rapeseed (as shown in Table 1). For sites A and B, rapeseed was sown in September, seedlings emerged in September-October, and the flowering period started in early March and ended in mid-April of the following year, so we selected sentinel-2 optical satellite images based on the rapeseed phenological period. To verify the robustness and Universal applicability of the method, the Mountain Winter Rapeseed Index (MWRI) was first established at points A and B respectively, and then the accuracy was evaluated separately.

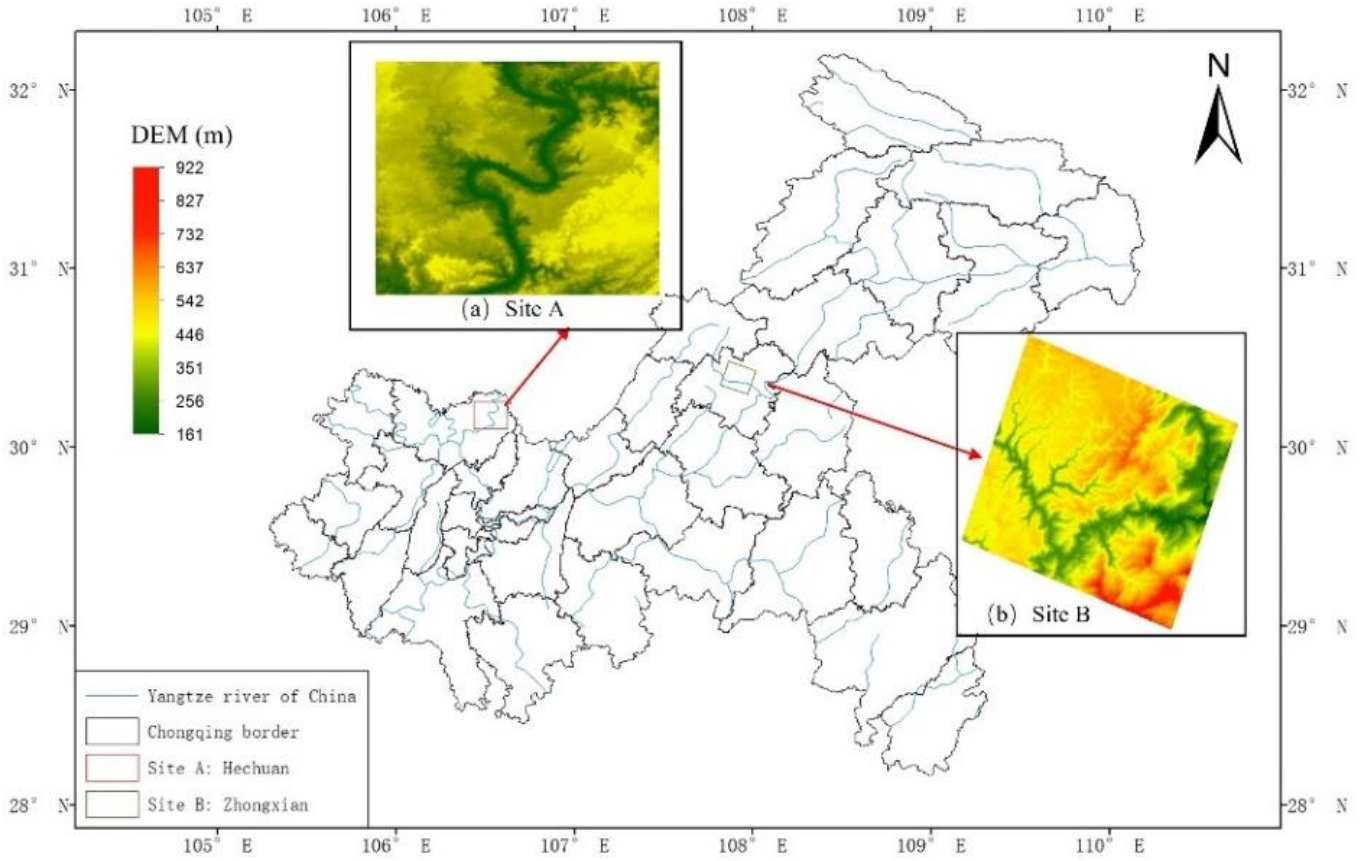

Figure 1. Locations of the study areas. (a) the position and terrain of sites A. (b) the position and terrain of sites B.

Table1. Phenological periods of major crops in the two study sites. A, and B represent site A, and site B, respectively. ①-⑪ represent the sowing, seeding, seedbed, transplant, early seedling, flower bud different, opening, bud, flowering, development, and maturity of the rapeseed growth period, respectively. ①-⑨ represent the sowing, seeding, three-leaf, tiller, jointing, booting, heading, and flowering, mature of the wheat growth period, respectively.

Table 1. Phenological periods of major crops in the two study sites.

Winter Rapeseed	A		①	②	③		④		⑤			⑥	⑦			⑧			⑨			⑩			⑪				
	B	① ②			③			④	⑤			⑥	⑦			⑧			⑨			⑩			⑪				
Winter wheat	A								①		②		③		④		⑤			⑥			⑦			⑧			⑨	
	B							①		②		③		④		⑤				⑥				⑦			⑧			⑨
Date		E	M	L	E	M	L	E	M	L	E	M	L	E	M	L	E	M	L	E	M	L	E	M	L	E	M	L	E	M	L
		Sep			Oct			Nov			Dec			Jan			Feb			Mar			Apr			May				
		Year												Year+1																

2.2 Optical Remote Sensing Data

Table 2 shows the time-series Sentinel-2 optical satellite images of the two study sites. Due to frequent rainy weather, the invalid images of continuous satellite sensor observations were filtered based on cloud cover information. Based on the phenological periods and visual interpretation shown in Table 1, we determined the flowering period of rape at sites A and B: 2020/02/16 - 2020/04/28 for site A and 2020/02/16 - 2020/05/18 for site B.

The optical satellite image "Sentinel-2" satellite was launched by ESA (European Commission and European Space Agency) [16]. The amount of image data is closely related to the spatial resolution [8]. Therefore, a large amount of data is encountered when analyzing Sentinel-2 images. The cloud computing platform of Google Earth Engine (GEE) provides a solution to handle the huge amount of remote sensing data [17]. GEE stores the complete data products from the world's most important remote sensing satellites (such as Sentinel) with good data management capabilities [18]. All Sentinel-2 images used in this study are from the image set "COPERNICUS/S2_SR" on the GEE platform, and the data from both sites cover the period from September 2019 to May 2020, and these images are all surface reflectance data that have been atmospherically corrected.

Although Sentinel-2 images cover 13 bands [19], crops are more sensitive in the red, green, blue, and near-infrared bands and two short-wave infrared bands, so we use these six bands of sentinel-2 as source image data and resample the short-wave infrared and near-infrared bands to 10 m resolution. In addition, we apply the F-mask algorithm [20] on the GEE cloud platform for cloud detection and cloud mask processing to remove the image elements covered by clouds, while these elements are no longer used for time series analysis and classification.

Table 2. Information of optical images used in this study.

Location	Acquisition date
Site A	10/19/2019 10/29/2019 12/10/2019 01/12/2020 02/16/2020 03/19/2020 04/28/2020 05/16/2020
Site B	09/26/2019 12/10/2019 03/19/2020 04/28/2020 05/03/2020 05/18/2020

2.3 Ground reference data

The ground truth data are derived from two datasets: the field survey samples and the Google Earth ultra-high resolution image dataset. These sample data were generated based on farmland data from the third land survey. Meanwhile, the collected sample dataset consists of 622 oilseed rape samples, 324 winter wheat samples, and 78 kale samples, and these crops have similar growth periods as rapeseed. samples from Site A are used to analyze the time series of several crops and to validate the extraction results of rapeseed; samples from point B are only used to evaluate the applicability of the proposed method on different cropping patterns/environments.

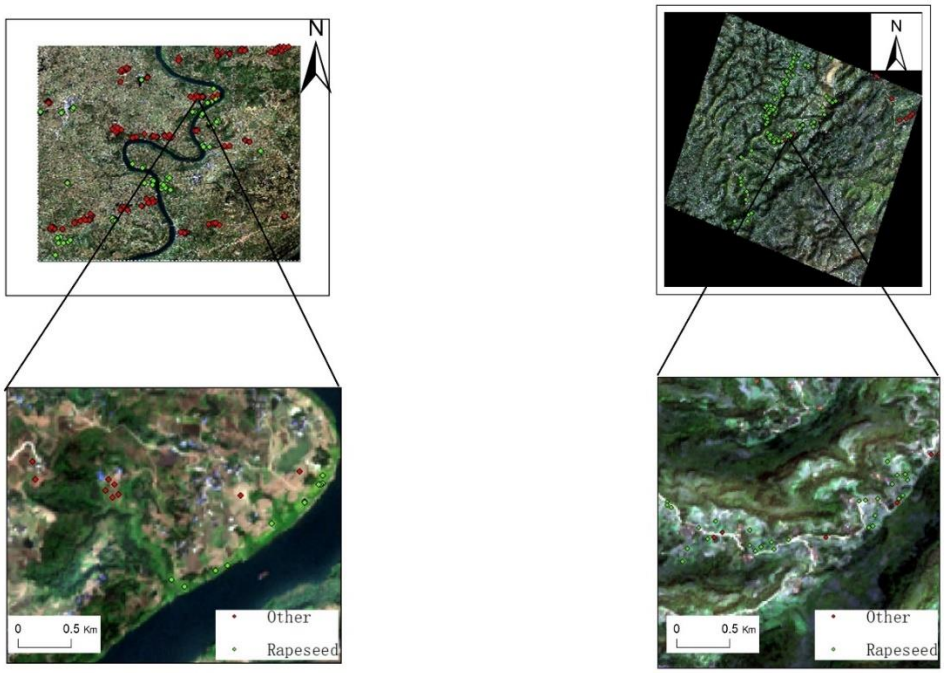

(a) (b)

Figure 2. Distribution of ground reference data. (a-b): Google Earth images and ROIs for sites A and B

3. Methods

We developed the MRM method based on site A and validated it at site B. The overall workflow is shown in Figure 3 and includes the following steps: (1) Preprocessing of optical-optical images using atmospheric correction and cloud detection algorithms; based on these preprocessed data and 30 m land cover products to obtain masks for irrigated farmland areas while focusing only on farmland for winter crops. (2) Based on this, a new rape index was designed to improve the reflection signal of rape during the flowering period. (3) A multi-classifier was used to achieve rape extraction in cloudy and rainy areas. (4) Finally, the results of rape mapping by MWRI and MRM were evaluated quantitatively using ground truth data. Furthermore, all steps were implemented under the GEE platform.

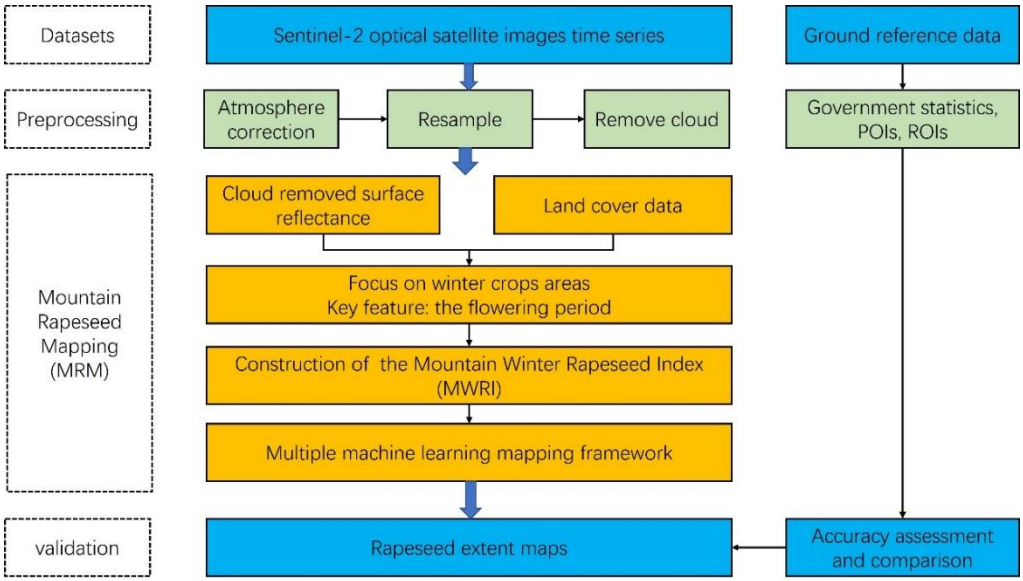

Figure 3. Overall workflow of this study.

3.1 Extraction of winter crops

When extracting crops from different land cover types, the phenomenon of "different spectra for the same thing, same spectrum for different things" may occur, i.e., one crop may show different spectra or different crops may have similar spectra, which may lead to false detection to some extent. The use of arable land plot masks to eliminate non-cropland is a typical strategy to solve this problem [21][22]. Liangyun Liu's team released the 2020 global 30-meter fine ground cover product [23] in 2021, which contains a total of 29 ground cover types and provides the latest data support for remote sensing agricultural applications. Based on this product, we obtained the irrigated farmland data of sites A and B through masks.

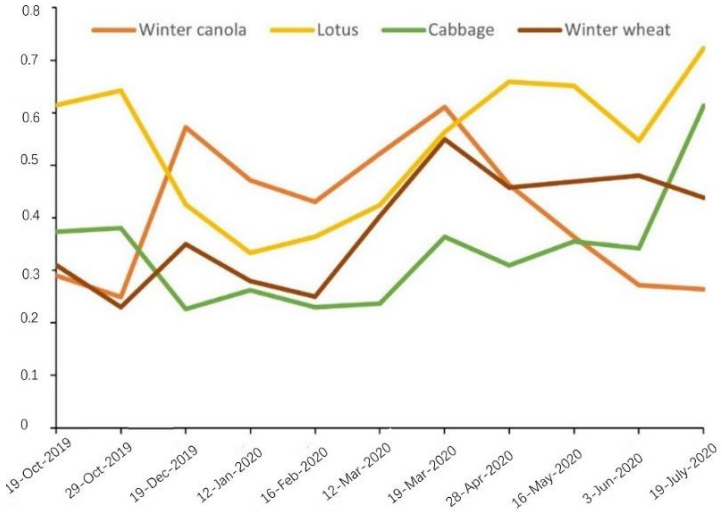

Figure 4. Time-series NDVI profiles

One of the most common methods to extract information on the distribution of winter crops is to use NDVI time series images to distinguish the phenological differences between winter and non-winter crops [24] [25]. Figure 5 shows the NDVI time series variation profiles for winter wheat, winter rape, kale, and lotus root in 2019-2020. In these collected data, NDVI values of winter rape and winter wheat from November 2019 to April 2020 (winter crop growth period) started to increase in December, reached a maximum in early March, and reached a minimum after flowering in mid-March; kale and lotus root non-winter crops were at a lower NDVI value during this period. Meanwhile, the NDVI values of winter crops during this reproductive period were generally greater than 0.4. Therefore, we could use the NDVI time series to extract winter crop areas. We used a nonlinear quadratic polynomial fit [26] to the NDVI time series from October to May for sites A, B, and C. The quadratic coefficients determine the direction and size of the opening of the fitted curve. A coefficient less than zero indicates that the land cover type with that attribute is a winter crop.

3.2 Construction of winter rape index

In this section, a new method of rape index generation is presented. Although cloud occlusion in optical satellite images is unavoidable, we assume that there are still some small cloud-free areas in a large cloudy region and rapeseed is grown in these areas. Therefore, for these cloud-free areas, rapeseed can be extracted using a phenology approach.

The key issue in extracting rapeseed based on phenology is to distinguish rapeseed from other

winter crops. In China, wheat is easily confused with rapeseed [27][28]. The mean temporal spectral reflectance profiles of 322 rapeseed poi and 160 wheat poi based on Sentinel-2 time series images are shown in Figs. 5(a) - (h), corresponding to the imaging dates of 19 October 2019 to 16 May 2020 at point A.

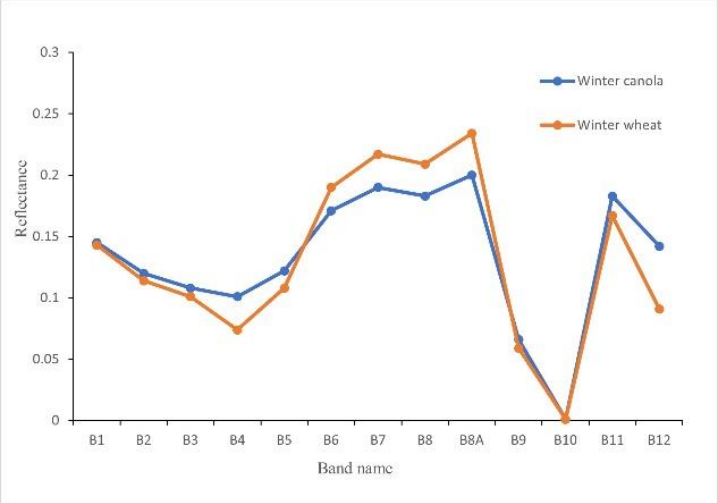

(a)

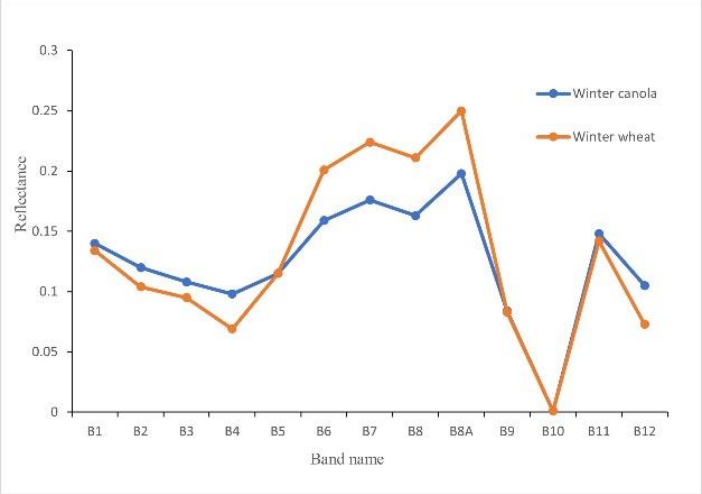

(b)

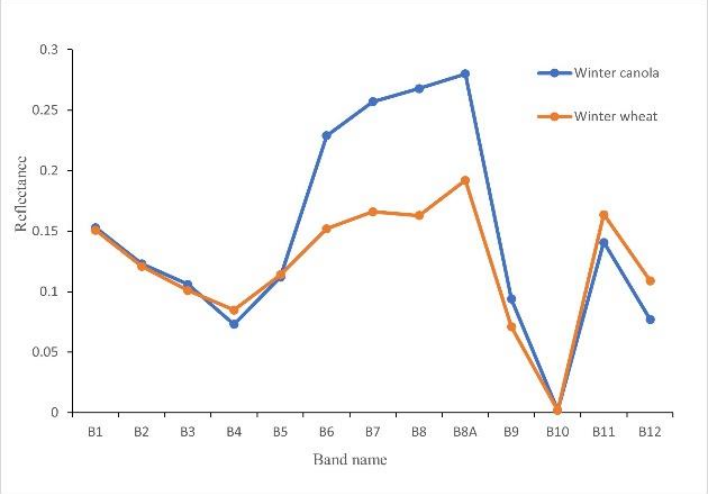

(c)

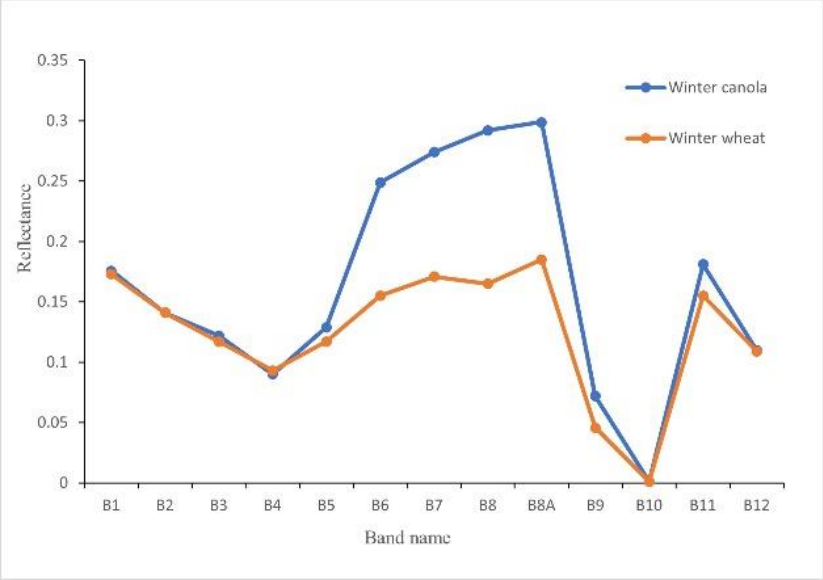
0.35
0.3
0.25
0.2
0.15
0.1
0.05
0
Reflectance
Winter canola
Winter wheat
B1 B2 B3 B4 B5 B6 B7 B8 B8A B9 B10 B11 B12
Band name

(d)

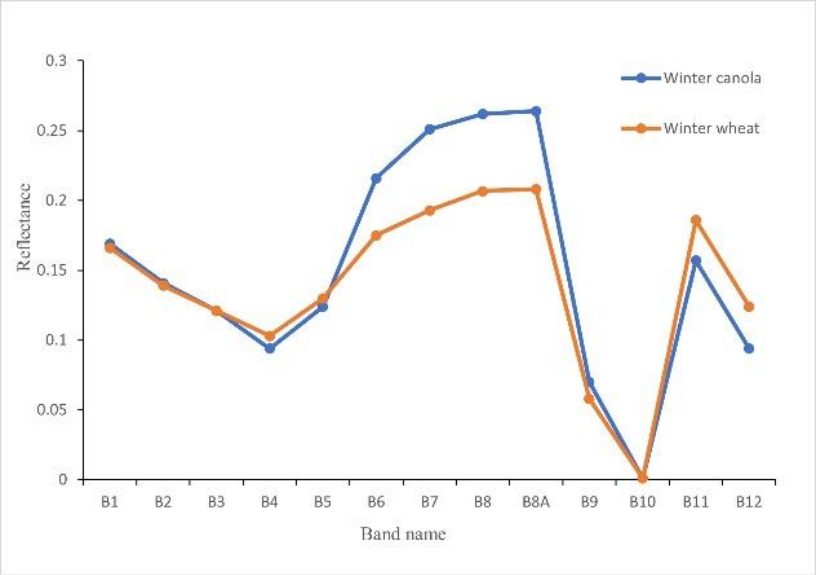
0.3
0.25
0.2
0.15
0.1
0.05
0
Reflectance
Winter canola
Winter wheat
B1 B2 B3 B4 B5 B6 B7 B8 B8A B9 B10 B11 B12
Band name

(e)

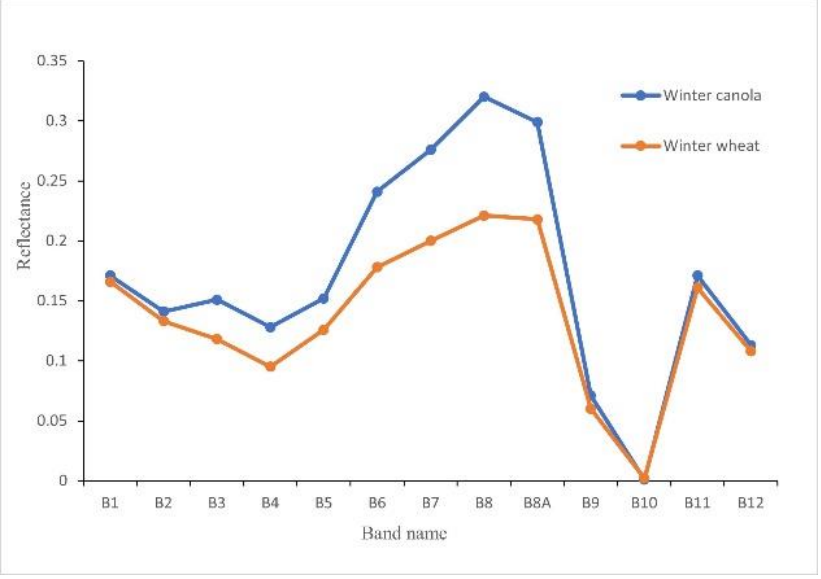
0.35
0.3
0.25
0.2
0.15
0.1
0.05
0
Reflectance
Winter canola
Winter wheat
B1 B2 B3 B4 B5 B6 B7 B8 B8A B9 B10 B11 B12
Band name

(f)

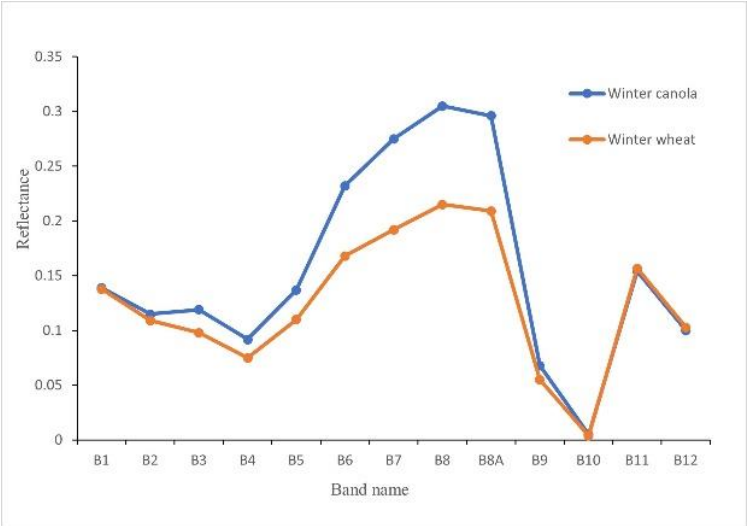

(g)

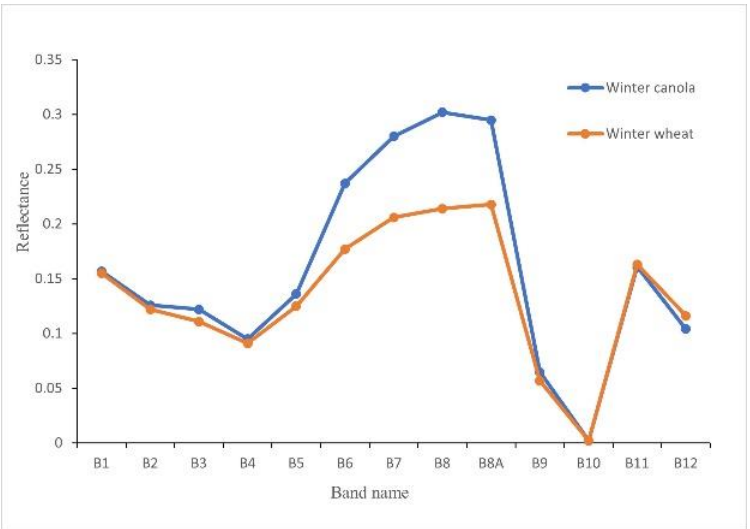

(h)

Figure 5. Time-series spectral curves of winter rapeseed and winter wheat.

Theoretically, the spectral reflectance difference between rapeseed and wheat is larger in the green (B3) and red (B4) bands, so features can be constructed to amplify the difference in spectral reflectance. However, as shown in Figure 5(c)-(e) during the bloom period (2020/02/01-2019/03/01), there is no significant difference between rapeseed and wheat in the green and red bands. the plot at point A is fragmented, and we speculate that this is the reason for the weaker signal of the rapeseed. Most previous rape phenology studies have confirmed the value of the visible band, and little attention has been paid to the phenological characteristics of rapeseed in the shortwave infrared band (SWIR). The SWIR1 band is less affected by the atmosphere and more sensitive to the water content of the soil or plants [29]. Considering the potentially different responses of the green/red band and SWIR1 band to the flowering process of rapeseed and wheat, we constructed the Mountain Winter Rapeseed Index (MWRI) by Eq. (1) to improve the differentiability of rapeseed

$$MWRI = \frac{\rho_{nir} - \rho_{green}}{\rho_{nir} + \rho_{green}} \times \frac{\rho_{swir1}}{\rho_{green} + \rho_{red}} \quad (1)$$

3.3 A multi-classifier-based framework for rapeseed identification

To verify whether MWRI enhances the image features of rapeseed compared with Sentinel-2 other rapeseed indices, MWRI images obtained based on Sentinel-2 original images and Sentinel-2 original images are extracted from rapeseed.

Machine learning can effectively control the convergence speed of the network, the risk of sample misclassification, and obtain the global optimal solution under small sample conditions, which has been widely used in remote sensing image classification and recognition research. The main classifiers include RF, SVM, and CART, and the performance of the classifiers has large differences under different conditions. Therefore, for the mountainous areas with complex rapeseed growing environments, we proposed the mountain rapeseed mapping method (MCM) to identify rapeseed growing information, i.e., a multi-classifier model was constructed in GEE using training samples and MWRI) to evaluate the performance of MWRI. As shown in Figure 6, this framework determines the optimal classifier to perform the classification based on the highest value of the F1-score of the accuracy rating metric obtained by different classifiers.

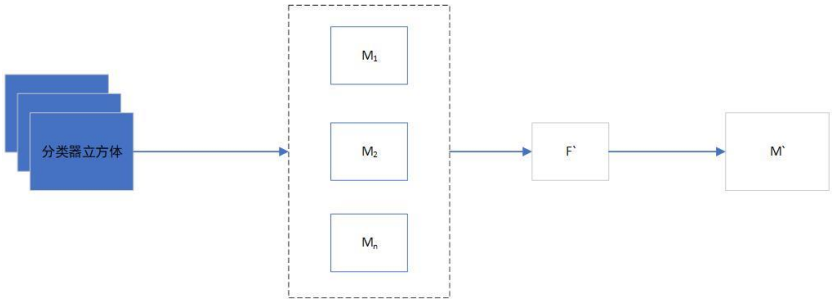

Figure 6. Multi-classifier fusion framework

where $M_{1\text{-}n}$ represents different classifiers and M' represents the optimal classifier. f' represents the F1-score.

3.4 Accuracy assessment of rapeseed mapping

We used the ground truth data described in Section 2.3 as a validation sample to assess the accuracy of rapeseed mapping. For the validation sample, we followed the non-proportional sampling allocation suggested by Olofsson et al [28] to increase the confidence in the accuracy assessment. The performance of the rapeseed mapping method was validated using the confusion matrix accuracy validation method and the F1 score. The confusion matrix accuracy parameters include overall accuracy (OA), production accuracy (PA), user accuracy (UA), and kappa coefficient. F1-score is a general validation metric that has been widely used in computer vision, especially in target detection tasks [30], as shown in Equation (2).

$$F1 - score = 2 * \frac{UA * PA}{(\mathrm{UA} + \mathrm{PA})} \quad (2)$$

In addition to pixel-based validation, we used agricultural statistics to assess the reasonableness of the area mapped for rapeseed throughout the study area. Agricultural statistics were obtained from the statistical yearbook published by the Chongqing Municipal Bureau of Statistics (http://tjj.cq.gov.cn/). The 2009-2021 Chongqing Statistical Yearbook records the annual acreage of grain and oil crops in each district and county of Chongqing.

3.5 Comparison of MWRI with other rapeseed indices

In previous studies, some rapeseed indices were used for rapeseed identification. For example, the Sulik and Long normalized difference yellowness index (NDYI) and yellowness index (RYI) with the following equations:

$$NDYI = \frac{f_{Green} - f_{Blue}}{f_{Green} + f_{Blue}} \quad (3)$$

$$RYI = \frac{f_{Green}}{f_{Blue}} \quad (4)$$

Among f_{Green} and f_{Blue} represent the green band and blue band of sentinel-2, respectively.

To compare the performance of the MWRI proposed in this study with the existing rapeseed indicators NDYI and RYI, their classification accuracies based on different classification methods were also obtained in this study.

4. Result

4.1 MWRI rapeseed identifiability

The Jeffries-Matusita (JM) distance method was chosen to assess the ability of different indices to differentiate between rapeseed and other crops. Table 3 calculates the JM distances between wheat to rapeseed for different indices at the four study sites based on an equal number of randomly selected samples (N = 200). JM distances ranged from 0 to 2. A JM distance of 2 meant that the two classes were 100% separable. Our proposed MWRI seemed to be the best indicator compared to NDYI, and RYI because it yielded the highest separability. For site A, the WRI and NDYI reached acceptable JM distance values (>1.7). For site B, MWRI, RYI, and NDYI reached acceptable JM distance values, but CI had less effect on JM distance.

Figure 6 depicts the time series profiles of different indices for wheat and rapeseed for all study sites. The MWRI time series curves showed an inverted "V" shape of increasing-decreasing throughout the rape growing season, with a positive peak in the rape MWRI index in mid-February 2020 and a positive peak in the other rape yellow flower indices in mid-March, which improved the identifiability of early rape. At the same time, the difference between the peak and minimum MWRI values of wheat compared with NDYI and RYI indices is obvious, which increased the distinguishability between winter rape and wheat.

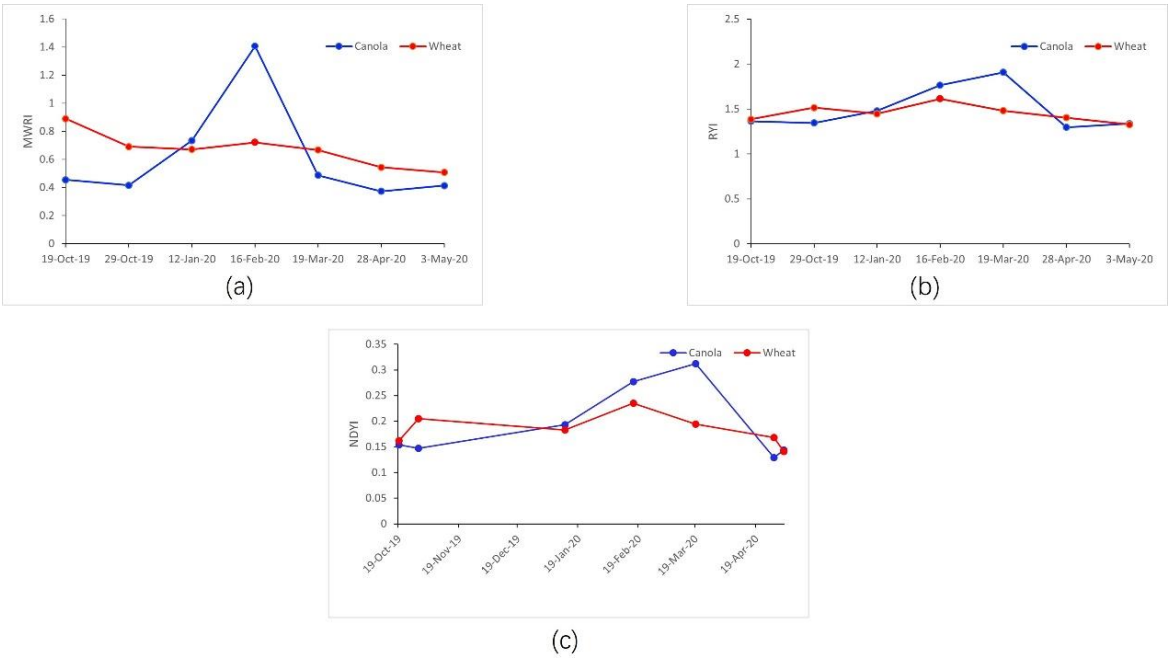

Figure 6. Time-series index curves of winter rapeseed and winter wheat.

（a）-（c）respect MWRI、RYI、NDYI time-series index curves.

Table 3. The value of JM distance for different indices in all two study sites.

Location	Index	Paris of crops	JM distance
Site A	MWRI	Rapeseed vs. Wheat	1.92
	NDYI	Rapeseed vs. Wheat	1.83
	CI	Rapeseed vs. Wheat	1.72
	RYI	Rapeseed vs. Wheat	1.748
Site B	MWRI	Rapeseed vs. Wheat	1.88
	NDYI	Rapeseed vs. Wheat	1.76
	CI	Rapeseed vs. Wheat	1.65
	RYI	Rapeseed vs. Wheat	1.72

4.2 Results and accuracy assessment of rapeseed identification

Based on the classification methods of WRI and MRM, we obtained the distribution map of rapeseed planting in 2020 at two sites, as shown in Figure 7. The planted area of rape at sites A and B is 18.23 km^2 and 2.67 km^2, respectively. rape at site A is mainly distributed in flat areas and valleys on both sides of the river, and the density scale of planting is larger. At Site B, rapeseed is distributed along roads and rivers, and the planting plots are more fragmented and dominated by small farmers.

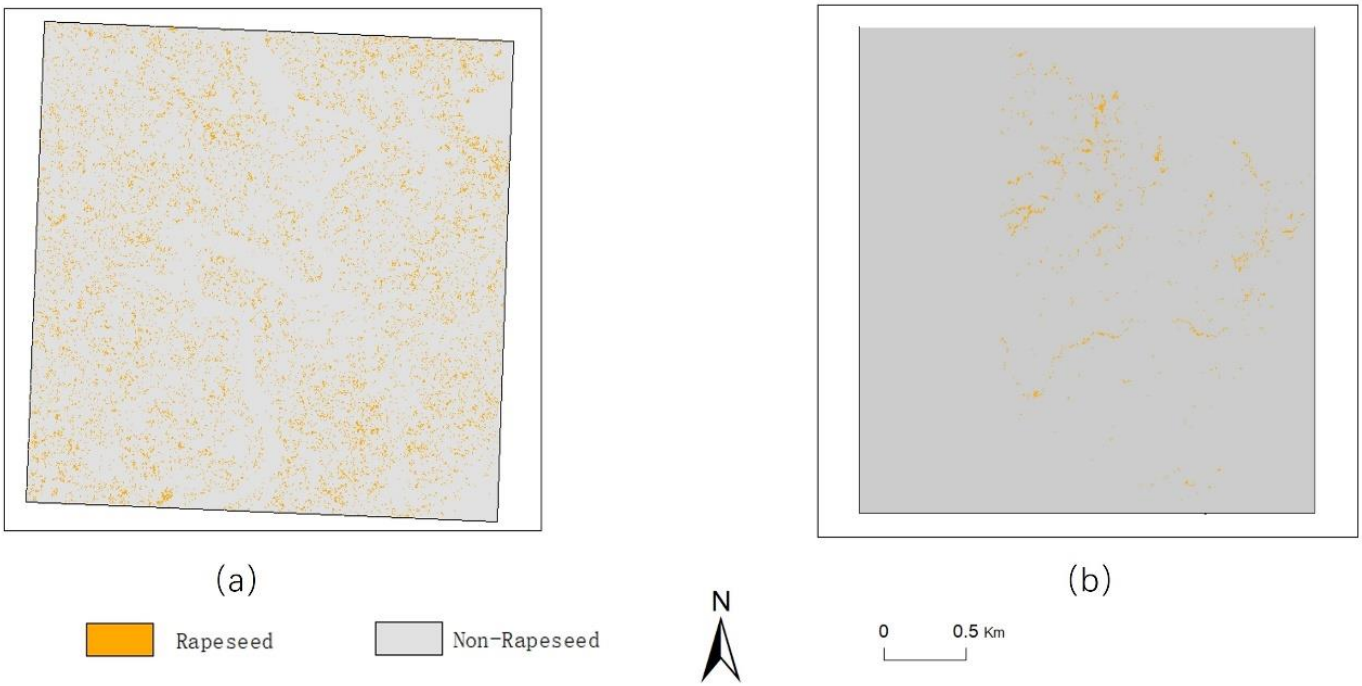

Figure 7. Spatial distribution of rapeseed based on WRI.

（a）and（b）represent rapeseed distribution in Site A and Site B, respectively

The classification accuracy results based on various existing rapeseed metrics using a multi-classifier fusion approach are shown in Table 4, where MWRI achieved the best results for identifying rapeseed in both study areas. For MWRI, its production accuracy for the rapeseed category was similar to its user accuracy for the rapeseed category. This indicates that the omission rate and misclassification rate of rapeseed are similar in the classification results based on MWRI images. These two errors would cancel each other out, making the area of rapeseed in the classification results closer to the real one. In terms of overall accuracy and kappa coefficient, the classification accuracy of NDYI is second only to MWRI, followed by RYI.

Table 4. Comparison of three rapeseed mapping indices.

Location	Metrics	MWRI-based	NDYI-based	RYI-based
Site A	OA (%)	97.54	95.74	92.31
	PA (%)	88.70	70.72	87.47
	UA (%)	92.81	92.46	92.90
	Kappa	0.8878	0.7780	0.8421
	F1-score	0.9071	0.6687	0.9017
	R^2	0.9529	0.8676	0.8330
Site B	OA (%)	96.28	86.87	87.44
	PA (%)	88.76	93.39	72.50
	UA (%)	84.11	52.52	74.35
	Kappa	0.8413	0.5988	0.6156
	F1-score	0.7950	0.5064	0.5799
	R^2	0.9701	0.6544	0.6067

Figure 8 shows the accuracy results of the partial validation samples at points A and B, which visually expresses the spatial distribution of classification accuracy. Misclassification occurs mainly in the boundary areas of each category. However, the interior of rapeseed plots can usually be accurately identified using the method proposed in this study. The area of rapeseed

classification results for each validation sample was compared with its true area on the ground, as shown in Figure 9. The results showed that the identified area of rapeseed was very similar to the ground truth area of rapeseed with a correlation coefficient of 0.9701. The production and user accuracies were also balanced, as shown in Table 7. Therefore, the identified area of rapeseed is very close to the real area.

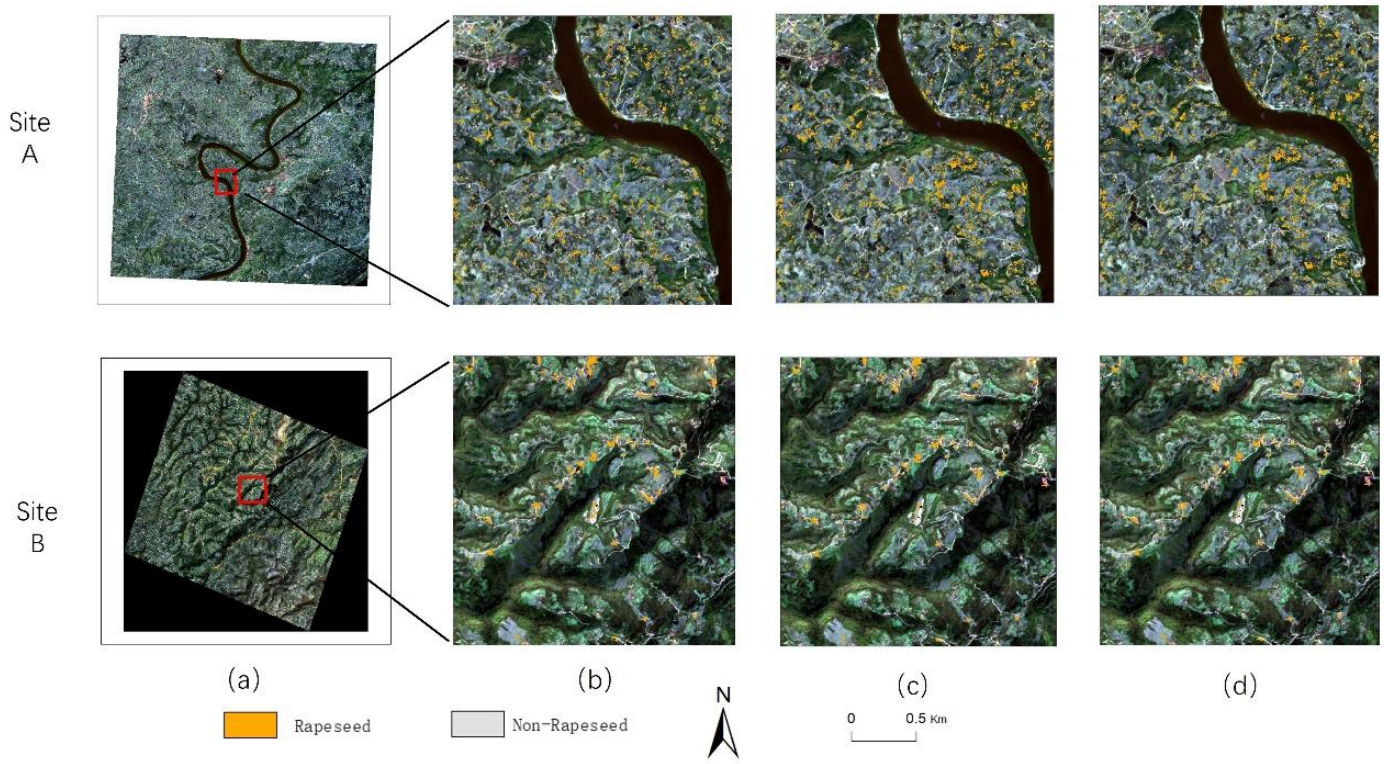

Figure8. Rapeseed maps in all study sites. (b)presents the (a) results of MWRI-derived rapeseed. (c) presents the (a) results of NDYI-derived rapeseed. (d) presents the (a) results of RYI-derived rapeseed.

5. Discussion

The ornamental value of rapeseed flowers and the oil extraction role of rapeseed increase the demand for rapeseed planting planning, so many existing studies have focused on the use of remote sensing technology to obtain information on the spatial distribution of rapeseed. Different from previous work on rapeseed mapping, this paper focuses on (1) proposing a new rapeseed index to enhance rapeseed signal based on irrigated farmland dataset, which improves the separability of rapeseed and wheat; (2) constructing a multi-classifier fusion framework with robustness for extracting rapeseed from time-series optical satellite images in complex scenarios.

5.1 Advantages of MWRI in rapeseed identification

In irrigated farmland, the spectral differences between rapeseed and winter wheat during peak growth are not significant. Wheat can severely reduce the mapping accuracy of rapeseed, especially in mixed wheat and rapeseed areas. However, yellow rape flowers provide another opportunity to distinguish rapeseed from winter wheat, but the rape flowering period belongs to the late stage of rape growth and being able to identify rape signals before rape flowering can improve real-time agricultural remote sensing. According to our observation, the yellow flowers of rapeseed can produce a visual distinction between rapeseed fields and winter wheat fields.

The greatest spectral differences between yellow and non-yellow petals are in the green and red bands. Rapeseed petals are high in carotenoids; they absorb blue light and reflect green and red light. At the vegetation canopy scale, spectral reflectance values were recorded from the yellow flowers and green leaves and stems of rapeseed. The values for other crops (winter wheat) came only from their green leaves and stems [10] [31]. The results showed that the spectral reflectance values of rapeseed in the red and green wavelengths during the flowering period were higher than those of other vegetation types. However, in the blue and near-infrared bands, the spectral reflectance values of rapeseed and wheat were similar. A decrease in soil and rapeseed moisture content during the flowering period would be observed using SWIR1. Therefore, the MWRI proposed in this study can be used to more accurately identify rape-growing areas.

5.2 The auxiliary role of multi-classifier fusion in rapeseed identification

Another problem we address is rapeseed extraction in complex scenes using time-series optical images. Rich machine learning classifiers support large-scale and long-term crop recognition. However, the features of the input classifiers are constrained by complex environmental factors, which leads to spatial variation in rapeseed recognition in complex scenes. We wish to develop a generalized optical satellite-influenced rapeseed mapping framework for rapeseed recognition in complex scenes. Therefore, we developed a multi-classifier fusion framework. The experimental results show that the method has high accuracy and stability, which is better than the single classifier method.

5.3 Limitations and Implications for Future Research

Despite these findings, the frequency of revisits and the number of high-quality images from optical satellite surveys should be considered when characterizing the peak of each indicator in rapeseed. Cloud occlusion is one of the main limitations for consistent and accurate detection of rapeseed bloom phenology. In this study, collecting samples still requires a lot of human and financial resources, but extracting the training samples corresponding to the feature attributes to the points to build a crop sample library will enable sample migration and provide a solid foundation for future research. Due to the increasing availability of high-quality images [32], especially from the European Sentinel-2 satellite, the new method of indexing proposed in this study will have great potential at low latitudes. We believe that evaluating the applicability of the method in different years to validate the feasibility of the method in this study and establishing a sample library of crop features for sample migration are important research directions in future studies.

6. Conclusion

We used the open-source platform GEE to access rich remote sensing images and data resources and used Sentinel-2 multispectral images to extract information on the spatial distribution of rapeseed in complex scenes. The spectral index MWRI proposed in this study is extremely sensitive to early rape flowers. Therefore, MWRI has great potential in accurately identifying the distribution of early rapeseed plantings. We conclude the following.

Early flowering of rapeseed is the best period for remote sensing data to identify its planting distribution, especially in the mixed cropping areas of different types of winter crops.

MWRI integrates four types of spectral information: green, red, near-infrared bands, and short-wave infrared bands. It greatly reduces the dimensionality and volume of remote sensing data, enhances the signal of winter rapeseed,

and improves the separability with winter wheat. Compared with other rapeseed indicators, the MWRI-based multi-classifier fusion framework can improve the classification accuracy of rapeseed. In addition, the framework model has good generality.

References

[1] X. Zhang, F. Liu, Y. He, and X. Gong, "Detecting macronutrients content and distribution in oilseed rape leaves based on hyperspectral imaging," *Biosyst. Eng.*, vol. 115, no. 1, pp. 56–65, 2013, doi: 10.1016/j.biosystemseng. 2013.02. 007.

[2] L. I. U. Cheng *et al.*, "Development present, potential and countermeasure of China oilseed rape industry" 2019.

[3] X. I. E. Hui, T. A. N. Tailong, L. U. O. Qing, Y. Liu, and C. Guanghui, "Development Status and Opportunities of Rape Industry," pp. 1–6, 2018.

[4] Yongxia Zhang, Feng Zhao, and Hongling Zhang, "Current situation, problems and countermeasure analysis of Chinese rape industry" World Agriculture, no. 04, pp. 96-99+203-204, 2015.

[5] J. J. Sulik and D. S. Long, "Spectral indices for yellow canola flowers," no. May, pp. 37–41, 2015, doi: 10.1080/01431161.2015.1047994.

[6] J. J. Sulik and D. S. Long, "Spectral considerations for modeling yield of canola ☆," *Remote Sens. Environ.*, vol. 184, pp. 161–174, 2016, doi: 10.1016/j.rse.2016.06.016.

[7] V. Data, "Remote Estimation of Vegetation Fraction and Flower Fraction in Oilseed Rape with Unmanned Aerial Vehicle Data," 2016, doi: 10.3390/rs8050416.

[8] M. Shen, J. Chen, X. Zhu, Y. Tang, and X. Chen, "Do flowers affect biomass estimate accuracy from NDVI and EVI?," *Int. J. Remote Sens.*, vol. 31, no. 8, pp. 2139–2149, 2010, doi: 10.1080 /01431160903578812.

[9] J. Tao, W. Wu, W. Liu, and M. Xu, "Exploring the spatio-temporal dynamics of winter rape on the middle reaches of Yangtze River Valley using time-series MODIS data," *Sustain.*, vol. 12, no. 2, 2020, doi: 10.3390/su12020466.

[10] D. Ashourloo *et al.*, "Automatic canola mapping using time series of sentinel 2 images," *ISPRS J. Photogramm. Remote Sens.*, vol. 156, no. July, pp. 63–76, 2019, doi: 10.1016/j.isprsjprs. 2019. 08.007.

[11] J. Han, Z. Zhang, and J. Cao, "Developing a New Method to Identify Flowering Dynamics of Rapeseed Using Landsat 8 and Sentinel-1/2," *Remote Sens.*, 2021.

[12] L. Blickensdörfer, M. Schwieder, D. Pflugmacher, C. Nendel, S. Erasmi, and P. Hostert, "Mapping of crop types and crop sequences with combined time series of Sentinel-1, Sentinel-2 and Landsat 8 data for Germany," *Remote Sens. Environ.*, vol. 269, no. December 2021, 2022, doi: 10.1016/ j.rse.2021.112831.

[13] S. Skakun *et al.*, "Early season large-area winter crop mapping using MODIS NDVI data, growing degree days information and a Gaussian mixture model," *Remote Sens. Environ.*, vol. 195, pp. 244–258, 2017, doi: 10.1016/j.rse.2017.04.026.

[14] Z. Liu *et al.*, "Plant Science Germinating seed can sense low temperature for the floral transition and vernalization of winter rapeseed (Brassica rapa)," *Plant Sci.*, vol. 307, no. March, p. 110900, 2021, doi: 10.1016/j.plantsci.2021. 110900.

[15] J. M. Peña-barragán, M. K. Ngugi, R. E. Plant, and J. Six, "Remote Sensing of Environment Object-based crop identi fi cation using multiple vegetation indices , textural features and crop phenology," *Remote Sens. Environ.*, vol. 115, no. 6, pp. 1301–1316, 2011, doi: 10.1016/j.rse.2011. 01.009.

[16] M. Drusch *et al.*, "Sentinel-2: ESA's Optical High-Resolution Mission for GMES Operational Services," *Remote Sens. Environ.*, vol. 120, pp.

25–36, 2012, doi: 10.1016/j.rse.2011.11.026.

[17] Q. Li, C. Qiu, L. Ma, M. Schmitt, and X. X. Zhu, “Mapping the land cover of africa at 10 m resolution from multi-source remote sensing data with google earth engine,” *Remote Sens.*, vol. 12, no. 4, pp. 1–22, 2020, doi: 10.3390/rs12040602.

[18] G. E. Engine, “Mapping of Land Cover with Optical Images, Supervised Algorithms, and Google Earth Engine,” pp. 1–19, 2022.

[19] S. M. Labib and A. Harris, “The potentials of Sentinel-2 and LandSat-8 data in green infrastructure extraction, using object based image analysis (OBIA) method,” *Eur. J. Remote Sens.*, vol. 51, no. 1, pp. 231–240, 2018, doi: 10.1080/22797254.2017.1419441.

[20] S. Qiu, Z. Zhu, and B. He, “Fmask 4.0: Improved cloud and cloud shadow detection in Landsats 4–8 and Sentinel-2 imagery,” *Remote Sens. Environ.*, vol. 231, no. May, p. 111205, 2019, doi: 10.1016/j.rse.2019.05.024.

[21] P. Defourny *et al.*, “Near real-time agriculture monitoring at national scale at parcel resolution: Performance assessment of the Sen2-Agri automated system in various cropping systems around the world,” *Remote Sens. Environ.*, vol. 221, no. March 2018, pp. 551–568, 2019, doi: 10.1016/j.rse.2018.11.007.

[22] Y. He *et al.*, “Examining rice distribution and cropping intensity in a mixed single- and double-cropping region in South China using all available Sentinel 1/2 images,” *Int. J. Appl. Earth Obs. Geoinf.*, vol. 101, p. 102351, 2021, doi: 10.1016/j.jag.2021.102351.

[23] X. Zhang, L. Liu, X. Chen, Y. Gao, S. Xie, and J. Mi, “GLC_FCS30: global land-cover product with fine classification system at 30 m using time-series Landsat imagery,” *Earth Syst. Sci. Data*, vol. 13, no. 6, pp. 2753–2776, Jun. 2021, doi: 10.5194/essd-13-2753-2021.

[24] L. Pan, H. Xia, X. Zhao, Y. Guo, and Y. Qin, “Mapping winter crops using a phenology algorithm, time-series sentinel-2 and landsat-7/8 images, and google earth engine,” *Remote Sens.*, vol. 13, no. 13, 2021, doi: 10.3390/rs13132510.

[25] H. Tian, N. Huang, Z. Niu, Y. Qin, J. Pei, and J. Wang, “Mapping winter crops in China with multi-source satellite imagery and phenology-based algorithm,” *Remote Sens.*, vol. 11, no. 7, pp. 1–23, 2019, doi: 10.3390/rs11070820.

[26] J. bin TAO, W. bin WU, Y. ZHOU, Y. WANG, and Y. JIANG, “Mapping winter wheat using phenological feature of peak before winter on the North China Plain based on time-series MODIS data,” *J. Integr. Agric.*, vol. 16, no. 2, pp. 348–359, 2017, doi: 10.1016/S2095-3119(15)61304-1.

[27] A. Veloso *et al.*, “Understanding the temporal behavior of crops using Sentinel-1 and Sentinel-2-like data for agricultural applications,” *Remote Sens. Environ.*, vol. 199, pp. 415–426, 2017, doi: 10.1016/j.rse.2017.07.015.

[28] H. Tian *et al.*, “A Novel Spectral Index for Automatic Canola Mapping by Using Sentinel-2 Imagery,” pp. 1–18, 2022.

[29] J. Han, Z. Zhang, and J. Cao, “Developing a New Method to Identify Flowering Dynamics of Rapeseed Using Landsat 8 and Sentinel-1/2,” Remote Sens., 2021.

[30] P. Olofsson, G. M. Foody, M. Herold, S. V. Stehman, C. E. Woodcock, and M. A. Wulder, “Good practices for estimating area and assessing accuracy of land change,” *Remote Sens. Environ.*, vol. 148, pp. 42–57, 2014, doi: 10.1016/j.rse.2014.02.015.

[31] N. Ghorbanzadeh, A. Salehi, H. Pourbabaei, A. A. S. Tolarod, and S. J. Alavi, “Spatial variability of soil microbial indices in common alder COMMON ALDER (Alnus glutinosa) stands using a geostatistical approach in northern Iran,” *J. For. Res.*, vol. 30, no. 2, pp. 679–688, 2019,

doi: 10.1007/s11676-018-0651-4.

[32] J. H. Wilson, “Separating Crop Species in Northeastern Ontario Using Hyperspectral Data,” pp. 925–945, 2014, doi: 10.3390/rs6020925.